Quantum calculation of cold-atom diffraction using periodic magnetic fields

Yin Hung,* Bradley Schuller,† John Giblin,‡ and Janine Shertzer
Department of Physics, College of the Holy Cross, Worcester Massachusetts 01610, USA
(Received 5 October 2005; published 29 June 2006)

When cold atoms approach a periodically magnetized surface, they are scattered by the effective repulsive potential $U(x,y)=\mu_B m_F g B(x,y)$. If the period a of the magnetized surface is larger than the de Broglie wavelength λ of the atoms, the atoms are diffracted. We have developed a method for calculating the location and intensity of the diffraction peaks using formal scattering theory. We solve the exact two-dimensional Schrödinger equation with the finite element method and calculate the scattering amplitude $f(\phi)$ using the integral formula; a plot of $|f(\phi)|^2$ provides a visualization of the diffraction pattern. By varying the experimental parameters within a realistic range, we predict the optimal conditions for observing atom diffraction.

DOI: 10.1103/PhysRevA.73.062722 PACS number(s): 34.10.+x, 02.70.Dh

I. INTRODUCTION

The ability to trap and manipulate ultracold atoms has resulted in renewed interest in atom optics. Atom optical devices have been proposed that are based on static electric and magnetic fields [1,2]. A promising scenario for observing atom diffraction is the use of a periodically magnetized surface as a grating [3,4]. Diffraction efficiencies have been calculated using the rigorous coupled-wave analysis method [5] and the thin phase grating approximation [6]. In this paper, we present a method for calculating the position and intensity of the diffraction peaks by a direct numerical solution of the Schrödinger equation.

Formal scattering theory provides a natural framework to study atom diffraction. The Schrödinger equation is solved numerically in cylindrical coordinates subject to the appropriate boundary conditions, and the full scattering wave function is then used in the integral formula for the scattering amplitude $f(\phi)$, where ϕ is the azimuthal angle. A plot of $|f(\phi)|^2$ indicates the angular distribution of the scattered particles. When the period a of the grating is larger than the de Broglie wavelength λ of the atoms, the atoms are diffracted.

In Sec. II, we review the theory of cold atom diffraction from periodically magnetized surfaces. In Sec. III, we provide details of the scattering calculation. The results and conclusion are given in Secs. IV and V, respectively.

II. COLD-ATOM DIFFRACTION FROM A MAGNETIZED SURFACE

In the proposed experiments, a cloud of cold-atoms at temperature T is released above a periodically magnetized surface. The magnetic field due to the surface decays exponentially with distance from the surface, and we assume the magnetic field is negligible in the region where the atoms are initially released. After falling a distance h, the atoms enter the magnetic interaction region with an initial velocity $v_{oy}=-\sqrt{2gh}$, where $|v_{oy}| \gg \bar{v}_T=\sqrt{3k_bT/m}$. In this region, the gravitational field can be neglected, and the potential is given by

$$U(x,y) = -\vec{\mu}\cdot\vec{B}(x,y). \tag{1}$$

If the direction of the magnetic field changes slowly enough, the magnetic moment will remain aligned with the field. The condition for adiabaticity is $|\vec{B}\times(\vec{v}\cdot\nabla\vec{B})|/B^2 \ll \omega$, where ω is the Larmor precession frequency. In the adiabatic picture, the potential for a particular magnetic sublevel m_F, $-F \le m_F \le F$, is given by

$$U(x,y) = \mu_B m_F g B(x,y), \tag{2}$$

where μ_B is the Bohr magneton and g is the Lande factor. We are interested in the case $m_F>0$, where the potential is repulsive.

The magnetic surface is constructed from a periodic array of ferromagnetically hard material in strips of thickness $\Delta x=\frac{1}{2}a$, with alternating magnetization. The maximum surface field is B_s. The magnetic surface lies in the $y=0$ plane. If we add a constant bias field $\vec{B}=B_b\hat{x}$ parallel to the surface, the resulting field above the surface is given by [3]

$$B(x,y>0) = \sqrt{B_b^2 + \tfrac{8}{\pi}B_bB_se^{-\kappa y}\cos(\kappa x) + \left(\tfrac{4}{\pi}B_s\right)^2 e^{-2\kappa y}}, \tag{3}$$

where $\kappa=2\pi/a$; the corresponding potential is

$$U(x,y) = \sqrt{U_b^2 + 2U_bU_se^{-\kappa y}\cos(\kappa x) + U_s^2e^{-2\kappa y}}, \tag{4}$$

where $U_b=\mu_B m_F g B_b$ and $U_s=\frac{4}{\pi}\mu_B m_F g B_s$. The role of the bias field is to provide the sinusoidal dependence in the potential. We consider the case where $U_s>K=\frac{1}{2}mv_{oy}^2>U_b$.

A full quantum treatment is needed only in the magnetic interaction region. Once the angular distribution of the diffracted atoms is known, the path of the atoms can be extrapolated using a classical trajectory, which includes the effects of the gravitational field.

*Current address: Harvard Medical School, Boston, MA 02115.
†Current address: Department of Nuclear Engineering, Massachusetts Institute of Technology, Cambridge, MA 02139.
‡Department of Physics, Yale University, New Haven, CT 06520.

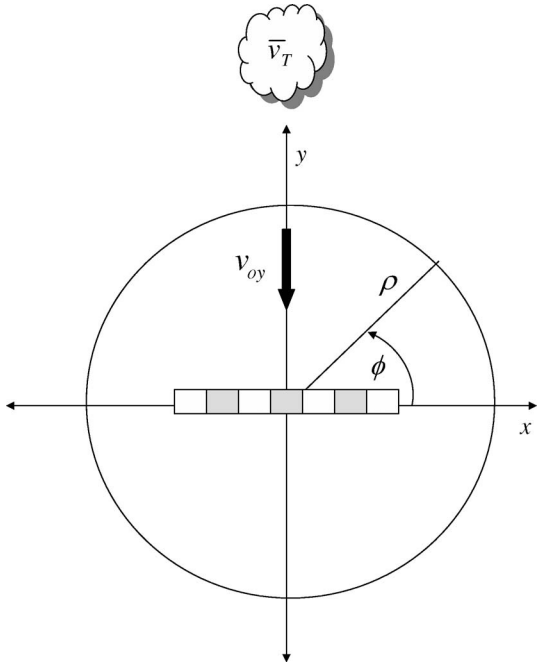

FIG. 1. The cloud of cold atoms is released above the periodically magnetized surface, which lies in the $x-z$ plane. The atoms enter the interaction region with initial velocity $v_{oy}=-\sqrt{2gh}$.

III. METHOD

We solve the Schrödinger equation in the interaction region, assuming plane wave incidence, which is valid as long as $|v_{oy}| \gg \bar{v}_T$. The problem is formulated in cylindrical coordinates (see Fig. 1). The full scattering wave function $\psi_k(\rho,\phi)$ is found by solving the two-dimensional (2D) time-independent Schrödinger equation

$$-\frac{\hbar^2}{2m}\left[\frac{\partial^2}{\partial\rho^2}+\frac{1}{\rho}\frac{\partial}{\partial\rho}+\frac{1}{\rho^2}\frac{\partial^2}{\partial\phi^2}\right]\psi_k(\rho,\phi)+U(\rho,\phi)\psi_k(\rho,\phi) - \frac{\hbar^2k^2}{2m}\psi_k(\rho,\phi)=0, \tag{5}$$

where $k=\frac{2\pi}{\lambda}=\frac{m|v_{oy}|}{\hbar}$. Assuming $U(\rho,\phi)$ vanishes at large ρ, the wave function obeys the asymptotic boundary condition

$$\psi_k \to e^{-ik\rho\sin\phi}+\frac{1}{\sqrt{\rho}}e^{ik\rho}f_k(\phi). \tag{6}$$

The solution of Eq. (5) yields the scattering wave function $\psi_k(\rho,\phi)$ and the scattering amplitude $f_k(\phi)$. The accuracy of the scattering amplitude obtained from a direct solution of Eq. (5) depends on how well the wave function is represented in the asymptotic region, where the wave function is highly oscillatory.

One can obtain more accurate and stable results for the scattering amplitude by using the wave function $\psi_k(\rho,\phi)$ in the integral formula for the scattering amplitude $f_k(\phi)$ [7]

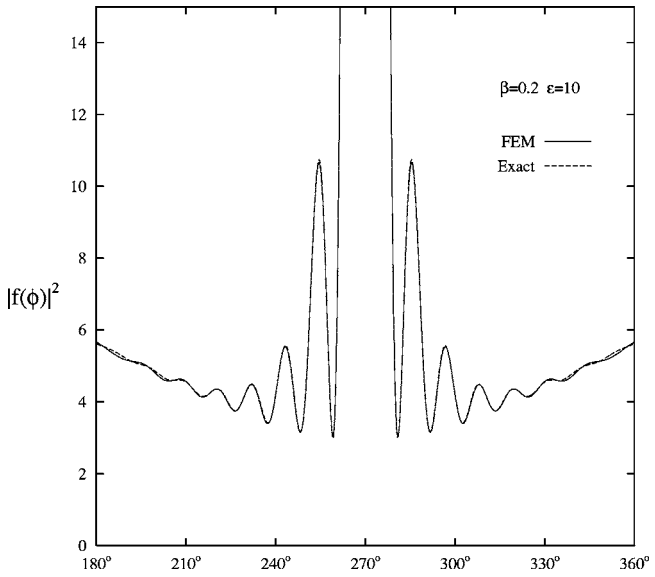

FIG. 2. $|f(\phi)|^2$ for a finite potential cylinder with $\beta=0.2$ and $\varepsilon=10$.

$$f_k(\phi)=-\frac{m}{\hbar^2\sqrt{2\pi k}}e^{i\pi/4} \times\int e^{-ik\rho'\cos(\phi-\phi')}U(\rho',\phi')\psi_k(\rho',\phi')\rho'd\rho'd\phi'. \tag{7}$$

In this case, the accuracy of the scattering amplitude depends on how well the wave function is represented in the interaction region.

In order to facilitate comparison with experiment we define the dimensionless variable $\xi=k\rho$ and the scaled potential $u(\rho,\phi)=\frac{U(\rho,\phi)}{K}$, where $K=\frac{\hbar^2k^2}{2m}$. Equation (5) can now be re-expressed as

$$-\left[\frac{\partial^2}{\partial\xi^2}+\frac{1}{\xi}\frac{\partial}{\partial\xi}+\frac{1}{\xi^2}\frac{\partial^2}{\partial\phi^2}\right]\psi(\xi,\phi)+[u(\xi,\phi)-1]\psi(\xi,\phi)=0, \tag{8}$$

where the k-independent wave function obeys the asymptotic condition

$$\psi(\xi,\phi)\to e^{-i\xi\sin\phi}+\frac{1}{\sqrt{\xi}}e^{i\xi}f(\phi); \tag{9}$$

$f(\phi)=\sqrt{k}f_k(\phi)$ is also independent of k.

The integral expression for the scaled scattering amplitude is given by

$$f(\phi)=-\frac{1}{\sqrt{8\pi}}e^{i\pi/4}\int e^{-i\xi'\cos(\phi-\phi')}u(\xi',\phi')\psi(\xi',\phi')\xi'd\xi'd\phi'. \tag{10}$$

With this change of variables, the scattering amplitude $f(\phi)$ is independent of the mass or initial velocity of the atoms.

We solve Eq. (8) with the finite element (FE) method [8]. Exploiting the symmetry of the Hamiltonian, the coordinate

space defined by $0 \le \xi \le \xi_{\max}$ and $\frac{\pi}{2} \le \phi \le \frac{3\pi}{2}$ is discretized into finite regions called elements. In each element, the wave function is approximated locally by a set of polynomial basis functions. We impose continuity of the wave function across element boundaries and require that $\psi(\xi_{\max}, \phi)$ satisfy Eq. (9). The solution of the resultant set of linear equations yields the scattering wave function $\psi(\xi, \phi)$ and $f(\phi)$. We then use $\psi(\xi, \phi)$ to recalculate the scattering amplitude $f(\phi)$ with the integral formula of Eq. (10). We systematically increase the number of elements until the scattering amplitude $f(\phi)$ is converged. For the largest runs, we used 12 800 elements, which is equivalent to over 200 000 local basis functions.

IV. RESULTS

A. Test case: Finite cylindrical potential

We first consider the case of atoms incident on a uniform cylindrical magnetic field; the axis of symmetry lies along the z axis. Although this case is not a realistic potential for experimental purposes, it is exactly solvable and allows us to verify that our method can resolve multiple diffraction peaks. The scaled potential is

$$u(\xi, \phi) = \begin{cases} \varepsilon & \xi \le \frac{\pi}{\beta} \\ 0 & \xi > \frac{\pi}{\beta}, \end{cases} \tag{11}$$

where $\varepsilon = \dfrac{U_s}{K} > 1$ and $\beta = \dfrac{\lambda}{a} < 1$.

The exact scattering amplitude is given by

$$f(\phi) = \sqrt{\frac{2}{\pi}} e^{3i\pi/4} \sum_{\nu=-\infty}^{\infty} i^{\nu} e^{i\nu\phi} \times \left[\frac{\sqrt{\varepsilon - 1} J_{\nu}\left(\frac{\pi}{\beta}\right) \dot{I}_{\nu}\left(\frac{\pi\sqrt{\varepsilon-1}}{\beta}\right) - \dot{J}_{\nu}\left(\frac{\pi}{\beta}\right) I_{\nu}\left(\frac{\pi\sqrt{\varepsilon-1}}{\beta}\right)}{\sqrt{\varepsilon - 1} H_{\nu}^{(1)}\left(\frac{\pi}{\beta}\right) \dot{I}_{\nu}\left(\frac{\pi\sqrt{\varepsilon-1}}{\beta}\right) - \dot{H}_{\nu}^{(1)}\left(\frac{\pi}{\beta}\right) I_{\nu}\left(\frac{\pi\sqrt{\varepsilon-1}}{\beta}\right)} \right], \tag{12}$$

where $J_{\nu}(x)$ is the Bessel function, $H_{\nu}^{(1)}(x)$ is the Hankel function of the first kind, and $I_{\nu}(x)$ is the modified Bessel function; $\dot{J}_{\nu}(x)$, $\dot{H}_{\nu}^{(1)}(x)$, and $\dot{I}_{\nu}(x)$ are the derivatives with respect to x.

In Fig. 2, we compare the exact results and the FE results for $|f(\phi)|^2$ for the case $\varepsilon = 10$ and $\beta = 0.2$. We show here only the forward scattering ($\pi \le \phi \le 2\pi$). There are five distinct diffraction peaks on either side of the large central peak at $\phi = \frac{3}{2}\pi$; the two lines are nearly indistinguishable. The back scattering $0 \le \phi \le \pi$ is relatively smooth and featureless. The FE calculation is able to reproduce even small features of the scattering amplitude, and provide sufficient resolution to locate all the diffraction peaks.

B. Potential due to a periodically magnetized surface

For the scattering calculations, we use a magnetized surface of *finite* width $w = \frac{1}{2}Na$, where N (odd) is the number of magnetized strips, arranged symmetrically about $x = 0$. It is necessary to use a finite size grating in order to impose the asymptotic boundary conditions. The weak bias field extends over the entire interaction region, and the scaled potential is given by

$$u(\xi, \phi) = \begin{cases} \varepsilon \sqrt{\gamma^2 + 2\gamma e^{-\beta\xi \sin\phi} \cos(\beta\xi \cos\phi) + e^{-2\beta\xi \sin\phi}} & y \ge 0,\ |x| < \frac{1}{4}Na \\ \varepsilon\gamma & \text{elsewhere,} \end{cases} \tag{13}$$

where $\gamma = \frac{U_b}{U_s}$. We have assumed that the magnetic surface is of negligible thickness and ignore the potential inside the ferromagnetic strips. This is completely valid, since the atoms are deflected long before they reach the surface.

In order for our calculation to be useful to experimentalists, we need to consider realistic values for $\varepsilon = \frac{U_s}{K}$, $\gamma = \frac{U_b}{U_s}$, and $\beta = \frac{\lambda}{a}$. The trap contains a cloud of cold Rb-87 atoms, slowed to temperatures on the order of 10 μK. The cloud is released from the trap, and the atoms fall about 10 mm towards the periodically magnetized surface. The atoms enter the interaction region with a vertical speed of several hundred mm/s ($K \approx 10^{-19}$ erg). This corresponds to a de Broglie wavelength on the order of ten nanometers ($\lambda \approx 10^{-6}$ cm). The bias field B_b is approximately 1 G ($U_b \approx 10^{-20}$ erg). The typical surface magnetic field B_s is between 100 G and 1000 G (10^{-18} erg $\le U_s \le 10^{-17}$ erg). This corresponds to a range $10 \le \varepsilon \le 100$ and $0.01 \ge \gamma \ge 0.001$. Currently, the best available magnetic materials for atom diffraction have a period of a micron or less (10^{-5} cm $\le a \le 10^{-4}$ cm). In this study, we investigate a range $0.4 \ge \beta \ge 0.05$.

We plot the scaled potential surface $u(\xi, \phi)$ for $\beta = 0.2$, $N = 7$, $\varepsilon = 10$, and $\gamma = 0.01$ in Fig. 3(a); we also show the potential surface for $\varepsilon = 100$, $\gamma = 0.001$ in Fig. 3(b) (truncated at $u = 10$). Note that the structure of the potential surface in Fig. 3(b) is nearly the same as in Fig. 3(a); the potential surface is merely shifted away from the magnetic surface. This is somewhat counterintuitive, because the sinusoidal term in Eq. (13) is multiplied by γ, and one might expect the oscillations to be less significant for $\gamma = 0.001$. However, it is the ratio $\frac{U_b}{K} = \varepsilon\gamma$ that determines the relative magnitude of the oscillations, and consequently, the amount of diffraction. This suggests that the diffraction patterns for the two cases, $\varepsilon = 10$, $\gamma = 0.01$, and $\varepsilon = 100$, $\gamma = 0.001$, should be very similar. The only difference is that the atoms reverse their direction further from the magnetic plate for $\varepsilon = 100$ and $\gamma = 0.001$. In

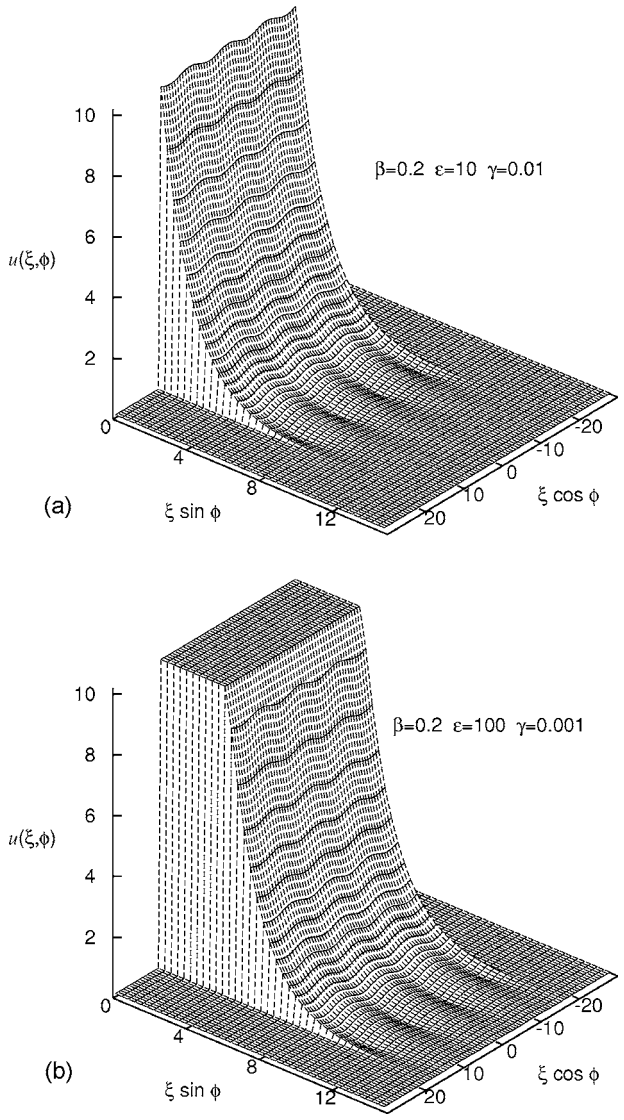

FIG. 3. Scaled potential due to a periodically magnetized surface (a) $\beta=0.2$, $\varepsilon=10$, $\gamma=0.01$; (b) $\beta=0.2$, $\varepsilon=100$, $\gamma=0.001$.

contrast, for $\varepsilon=10$ and $\gamma=0.001$ (not shown), the oscillations in the potential surface are barely visible; in this case, no diffraction of the atoms was observed.

In the actual experiment, the size of the atomic cloud is much smaller than the width of the grating, and all of the atoms in the cloud are back scattered (reflected). In the scattering calculation, we use a grating of finite width w and an incident plane wave. This results in both forward and backward scattering. In order to determine how the shape and relative amplitude of the back-scattered peaks vary with the experimental parameters, we have normalized the results such that $\int_0^\pi |f(\phi)|^2 d\phi=1$.

In Fig. 4, we show a plot of $|f(\phi)|^2$ for $\beta=0.4$. As expected, the peaks become much sharper as we increase N from 3 to 11, although the center of the peaks is unchanged. The diffraction patterns for $\varepsilon=10$, $\gamma=0.01$, and $\varepsilon=100$, $\gamma=0.001$ are similar. The primary diffraction maxima are located (approximately) at $\phi=\frac{1}{2}\pi\pm\sin^{-1}(n\beta)$, $n=0$, and 1. The second order peak is not observed. The fine structure superimposed on the primary diffraction pattern is not a numerical artifact. Rather, these secondary diffraction minima/maxima are associated with the finite width of the grating $w=\frac{1}{2}Na$. As we increase N, the structure becomes more complex and the secondary diffraction minima can distort the shape of a primary diffraction peak. However, because the primary peaks increase dramatically in amplitude, the secondary peaks become negligible for large N.

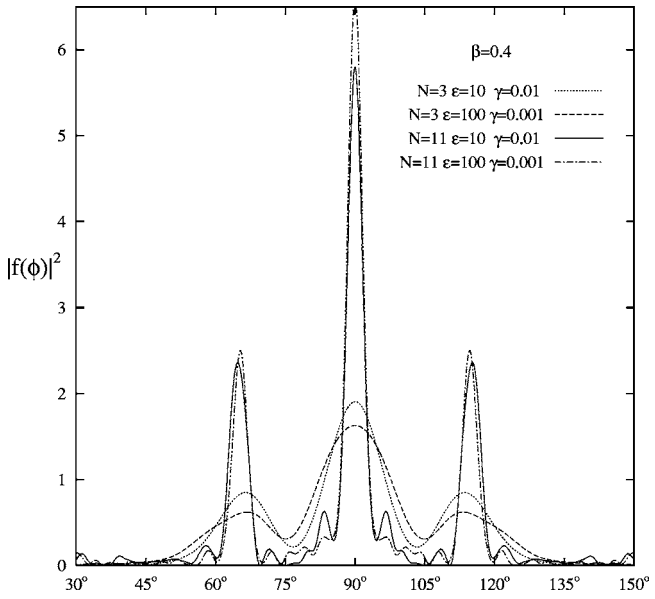

FIG. 4. $|f(\phi)|^2$ for a periodically magnetized surface with $\beta=0.4$.

In Figs. 5 and 6, we show the diffraction patterns for $\beta=0.3$ and $\beta=0.2$. There is a gradual suppression of the central peak. At $\beta=0.3$, the first order diffraction peaks are comparable in height to the central peak. With increasing N,the peaks become sharper. At $\beta=0.2$, the primary diffraction

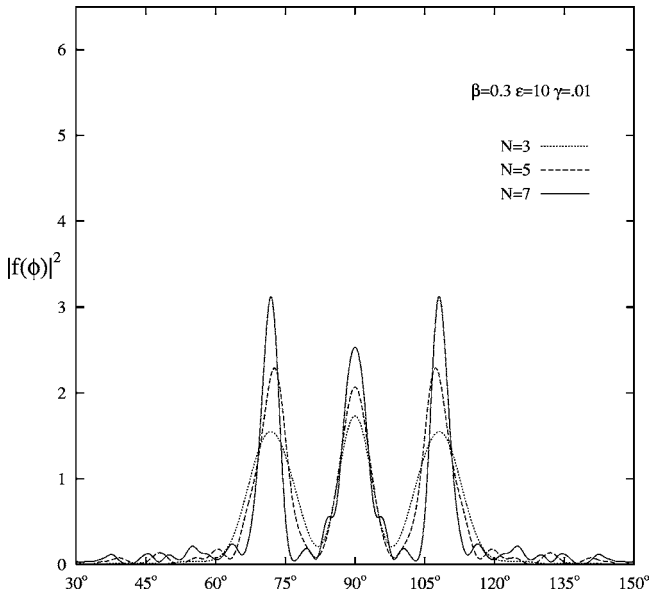

FIG. 5. $|f(\phi)|^2$ for a periodically magnetized surface with $\beta=0.3$.

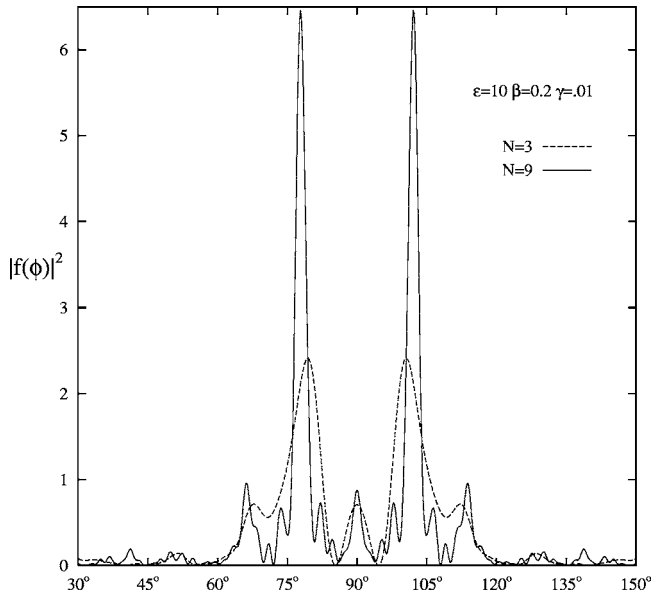

FIG. 6. $|f(\phi)|^2$ for a periodically magnetized surface with $\beta=0.2$.

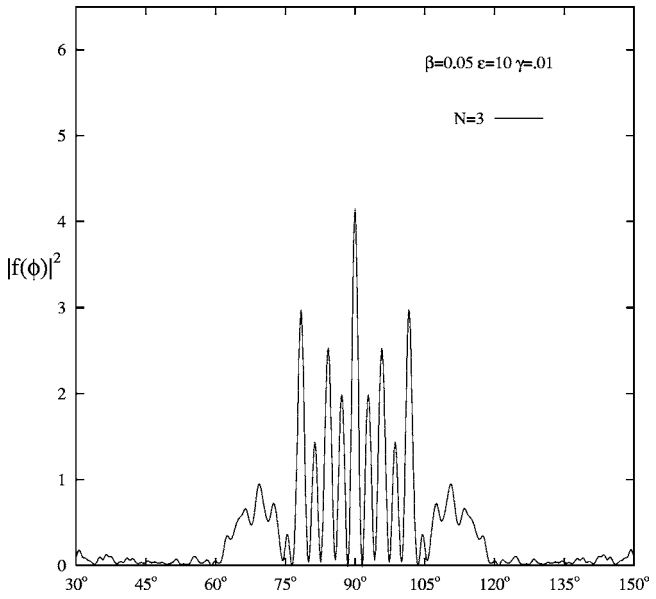

FIG. 8. $|f(\phi)|^2$ for a periodically magnetized surface with $\beta=0.05$.

maxima corresponding to $n=0$ and $n=2$ are almost completely suppressed; the first order diffraction peak $n=1$ is extremely sharp.

At $\beta=0.1$ (see Fig. 7), the central peak is again prominent. For $N=3$, there are seven distinct peaks ($n=0,1,2,3$); the peak associated with a particular odd n is more prominent than the $(n-1)$ peak. For $N=5$, the $n=4$ peaks are resolved. The $n=1$ peak has a pronounced dip at the center due to a secondary diffraction minimum associated with the finite width of the grating; this disappears at higher N.

At $\beta=0.05$ (see Fig. 8), there are nine distinct peaks for $N=3$. The even n peaks are dominant. At higher N (not shown), additional diffraction peaks can be resolved in the range $60°-75°$ and $105°-120°$. Since the angular spacing between the diffraction peaks is about 3°, this is probably a realistic lower limit for β for experimental purposes.

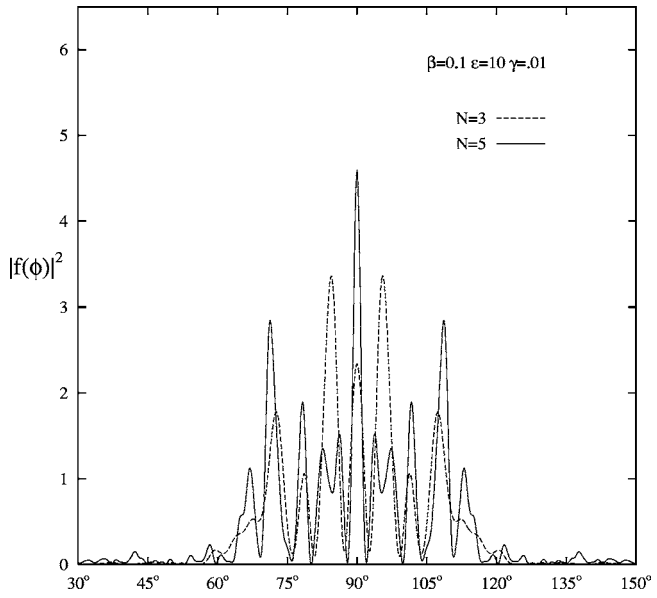

FIG. 7. $|f(\phi)|^2$ for a periodically magnetized surface with $\beta=0.1$.

V. CONCLUSION

Based on this study, we can make the following generalizations concerning the diffraction of cold atoms from a periodically magnetized surface. First, the ratio $\frac{U_b}{K}=\varepsilon\gamma$ determines whether the oscillations in the potential surface are sufficiently large to produce atom diffraction. Second, no primary diffraction peaks associated with the periodic structure of the grating are observable outside the cone $\phi=\frac{1}{2}\pi\pm\frac{1}{6}\pi$. Within that cone, the location of the primary diffraction *maxima* are given, to a reasonable approximation, by $\phi\approx\frac{1}{2}\pi\pm\sin^{-1}(n\beta)$. Third, the relative amplitude of the peaks change with increasing β; in some cases, the central peak is strongly suppressed. Fourth, the finite width of the grating leads to secondary diffraction peaks but *does not change the location of the primary peaks*. Increasing N decreases the width and increases the height of the diffraction peaks.

In conclusion, we have clearly established a range of parameters for which experimental observation of atom diffraction should be viable. Values of β for which either the even or odd n peaks are suppressed (e.g., $\beta=0.2$), are particularly promising candidates for diffraction detection.

ACKNOWLEDGMENTS

We are grateful to Timothy Roach for suggesting this problem and for many helpful discussions. We also thank Russell McLean and Timothy Roach for providing us with their experimental parameters. We are grateful to Alex Dalgarno for reading early drafts of this paper and offering many helpful suggestions.

[1] T. M. Roach, H. Abele, M. G. Boshier, H. L. Grossman, K. P. Zetie, and E. A. Hinds, Phys. Rev. Lett. **75**, 629 (1995); I. G. Hughes *et al.*, J. Phys. B **30**, 647 (1997); **30**, 647 (1997); **30**, 2119 (1997); C. V. Saba, P. A. Barton, M. G. Boshier, I. G. Hughes, P. Rosenbusch, B. E. Sauer, and E. A. Hinds, Phys. Rev. Lett. **82**, 468 (1999); A. I. Sidorov *et al.*, Quantum Semiclassic. Opt. **8**, 713 (1996); E. A. Hinds and I. G. Hughes, J. Phys. D **32**, R119 (1999).

[2] P. Rosenbusch *et al.*, Phys. Rev. A **61**, 031404(R) (2000).

[3] G. I. Opat *et al.*, J. Opt. B: Quantum Semiclassical Opt. **1**, 415 (1999).

[4] A. I. Sidorov *et al.*, Acta Phys. Pol. B **33**, 2137 (2002).

[5] T. J. Davis, Eur. Phys. J. D **14**, 111 (2001).

[6] T. J. Davis, Eur. Phys. J. D **14**, 289 (2001).

[7] J. Shertzer and A. Temkin, Phys. Rev. A **63**, 062714 (2001); J. Shertzer and A. Temkin, *ibid.* **70**, 042710 (2004).

[8] K. J. Bathe, *Finite Element Procedure in Engineering Analysis* (Prentice-Hall, Cliff, New Jersey, 1982).